energy&fuels

pubs.acs.org/EF
Article

Computational Co-optimization of Fuel and Spark-Ignition Engine

Published as part of Energy & Fuels special issue "Accelerating the Energy Transition: Advancements in Electrofuels".

Philipp Ackermann, Benjamin Auer, Patrick Burkardt, Bastian Lehrheuer, Philipp Morsch, Karl Alexander Heufer, Stefan Pischinger, Alexander Mitsos, and Manuel Dahmen*

Cite This: *Energy Fuels* 2025, 39, 4079–4093

ABSTRACT: Spark-ignition engine efficiency can be increased by co-optimizing fuel and engine. First, computational fuel design can optimize fuel molecules or composition using predictive fuel property models, e.g., for high octane numbers. Then, the engine configuration can be optimized experimentally to maximize the achievable efficiency. However, such a sequential co-optimization based on fuel properties may yield suboptimal fuels, as the fuel properties do not fully capture the complex fuel−engine interaction. Therefore, we propose the computational, simultaneous co-optimization of fuel and engine. To this end, we derive a thermodynamic engine model that predicts the engine performance as a function of fuel composition and engine configuration. We calibrate the engine model against experimental data from a single-cylinder research engine, such that new candidate fuels require no model recalibration with additional experimental engine data. As a case study, we select 10 possible alternative fuel components identified in previous studies and create 39 binary and 60 ternary fuel mixtures. The composition of each fuel mixture is then co-optimized together with the compression ratio and the intake pressure of the engine considering knock and peak pressure constraints to ensure smooth and safe engine operation. The study reveals the small esters methyl acetate and ethyl acetate as promising fuel candidates for future spark-ignition engines. For methyl-acetate-rich blends, the engine model predicts knock-free operation at compression ratios of up to 20 and boost pressures of up to 1.8 bar, rendering methyl acetate a promising alternative to methanol. Considering significant model uncertainties, however, the findings require experimental validation.

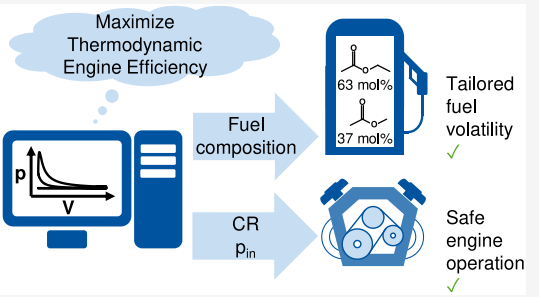

INTRODUCTION

Spark-ignition (SI) engines running on liquid fuels are central to today's mobility. Despite their technological maturity, they can still be improved in terms of efficiency.[1,2] The thermodynamic efficiency of SI engines increases with the compression ratio and, in general, with boosting pressure.[3] However, both high compression ratios and high boosting pressures lead to higher in-cylinder temperature and pressure. These extreme conditions may trigger autoignition of the fuel, leading to engine knock, which impairs engine operation and possibly damages the engine.[4] Increasing the thermodynamic efficiency by means of increasing compression ratio and boosting pressure requires lowering the autoignition propensity of the fuel.[5]

Traditionally, fuel autoignition propensity is rated by octane numbers like the research octane number (RON)[6] and the motor octane number (MON).[7] For both numbers, standardization organizations have established minimal acceptable values for marketed gasoline fuels to ensure knock-free operation in commercially used engines.[8,9] For modern, highly boosted SI engines, a high octane number alone does not describe the ignition propensity of a fuel sufficiently well.[10] In the early 2000s, the octane index (OI) was established as a more accurate measure for ignition propensity of gasoline fuels in modern SI engines.[11] The OI is defined as a weighted sum of RON and the octane sensitivity (OS). OS is defined as the difference between RON and MON[12] and its influence on OI is weighted with an empirical factor K.

Alternative fuels can enable higher compression ratios and boosting pressures than a typical RON 95 gasoline and thus higher thermodynamic efficiencies. A multitude of alternative fuels have been investigated in research engines and have achieved higher engine efficiencies than RON 95 gasoline. Examples for pure-component fuels include methylfuran,[13] 2-methylfuran,[14] 2-butanone,[14−16] methanol,[17−20] and ethanol.[14−17,21,22] Examples of multicomponent fuels include a

Received: September 30, 2024
Revised: January 31, 2025
Accepted: February 5, 2025
Published: February 12, 2025

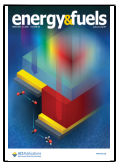

https://doi.org/10.1021/acs.energyfuels.4c04775
Energy Fuels 2025, 39, 4079−4093

blend of acetone, butanol, and ethanol,[23,24] a blend of ethanol, 2-butanone, cyclopentane, and cyclopentanone,[15,16,25] and a six-component blend containing a ketone, esters, alcohols, and an alkane (KEAA).[16,25] The experimental findings demonstrate the potential of alternative fuels to exploit advanced engine concepts. In all cases, the efficiency increase can be at least partly attributed to the lower autoignition propensity of the alternative fuels, which is reflected in high values of RON and OS of these fuels.

To unlock the full potential of both advanced engine concepts and alternative fuels, researchers have proposed systematic strategies to jointly develop engines and fuels, resulting in a co-optimization.[26−28] The maximization of thermodynamic efficiency includes numerous degrees of freedom that range from fuel constituents and composition to engine design and operation. Exploring this design space solely by extensive experimental investigations is prohibitive. The number of degrees of freedom can be reduced by means of computer-aided product design (CAPD).[29] CAPD identifies promising fuel components and blends using predictive property models.

Numerous studies have applied CAPD to fuels for advanced SI engines by targeting molecules and mixtures with high RON.[27,30−34] Alternative fuels designed in this manner have been experimentally investigated in single-cylinder research engines with high compression ratios and under highly boosted conditions.[14−16] The experimental investigations confirm the hypothesis that fuels with higher RON values enable thermodynamic efficiency increases. However, the maximization of RON does not necessarily lead to the maximization of thermodynamic engine efficiency. For example, 2-butanone exhibits a slightly higher RON than ethanol, but engine experiments report equal or higher thermodynamic efficiencies for ethanol.[14−16,25]

Fuel design can target OI instead of RON as an alternative objective[35] that incorporates the OS. The influence of the OS on the OI, however, depends upon the engine design and operating conditions, which are captured by an empirical factor K. The K factor is linked to high uncertainty in highly boosted engine operation[36] and itself depends upon the fuels used in its determination.[37] Furthermore, autoignition propensity is not the only fuel property that influences engine efficiency. A high enthalpy of vaporization can provide an additional efficiency increase through increased charge cooling during fuel evaporation. Charge cooling reduces both the wall heat losses and the combustion temperature, and thus results in higher thermodynamic efficiency and lower autoignition propensity.[38] The charge cooling effect is especially pronounced in light alcohol fuels such as methanol and ethanol.[17] However, its influence on the engine efficiency increase is challenging to isolate.[2]

Several models attempt to incorporate the charge cooling effect and further fuel properties in the prediction of achievable engine efficiency. Leone et al.[39] correlated the thermodynamic efficiency of gasoline−ethanol blends to octane number and ethanol content. The correlation has been used to design gasoline−ethanol blends,[40] but by its nature it is not applicable to alternative fuels other than ethanol. Szybist et al.[2] introduced the so-called engine efficiency merit function that correlates thermodynamic efficiency to fuel properties such as RON, OS, enthalpy of vaporization, and laminar burning velocity.[2] The merit function has been used in database screenings[33,41,42] and in a molecular design study of pure components and binary blends.[43] The authors of the merit function, however, discuss several limitations that compromise the utility of the function in computational co-optimization of fuel and engine.[2] With individual terms for the contribution of each fuel property to the thermodynamic efficiency, the merit function neglects the synergistic effects of the fuel properties on each other, e.g., the effect of the enthalpy of vaporization on the RON[44] or the OS.[45] Furthermore, the inclusion of the OS requires choosing a value for the K factor, introducing the same uncertainties as in the case of the OI, as discussed above. Importantly, the merit function does not provide direct information about engine conditions necessary to maximize the thermodynamic efficiency.

Zero-dimensional thermodynamic engine models constitute a more rigorous option for predicting thermodynamic efficiency, as they build on mechanistic knowledge. Moreover, they provide insight in how engine design and operation affect engine performance. Most engine modeling efforts have been restricted to specific engine designs with specific alternative fuels such as methanol,[46−49] hydrogen,[50] or hydrogen−methane mixtures.[51,52] Only few studies have used models to compare a limited number of fuels, but with calibrated parameter data for each fuel based on dedicated engine data.[53,54] The most comprehensive study has been published by Gschwend et al., who developed a dedicated thermodynamic engine model with an embedded optimization of the compression ratio[55] to evaluate alternative fuels and screened a database of 50 possible alternative fuel candidates for thermodynamic engine efficiency.[56] However, the existing engine models are not suited for computational co-optimization of fuels and engines maximizing engine efficiency as a function of fuel composition as well as engine design and operation, as they are either tailored to specific fuels and engine designs[46−52] or have not been validated for extreme engine conditions and alternative fuels.[53−55]

The present work provides a first approach to computational co-optimization of multicomponent fuels and SI engine configuration at stoichiometric combustion conditions to achieve maximum thermodynamic engine efficiency. As a central building block, we derive a predictive one-zone thermodynamic model of a single-cylinder research SI engine and implement it in MATLAB R2020a.[57] We calibrate and validate the model with measurement data of different alternative fuels and different compression ratios from a single-cylinder research engine. Notably, the model can be applied to new fuel candidates without the need for recalibration. Utilizing the model, we establish a computational co-optimization procedure of multicomponent fuels and SI engine configuration. First, we select few possible fuel constituents as candidates for blending based on previous CAPD studies. Then, we maximize the thermodynamic efficiency of the engine by varying the compression ratio, the intake pressure, and the fuel composition. The optimization is subject to knock and peak pressure constraints as well as volatility related fuel specifications.

The remainder of this article is structured as follows. First, the thermodynamic engine model is described, including its validation against experimental data. Then, the co-optimization of fuel and engine is described, including problem formulation (scope, constraints, and solution procedure), the resulting blends and their corresponding engine designs are discussed, and the predicted efficiencies are compared to RON, OI, and merit function values.

https://doi.org/10.1021/acs.energyfuels.4c04775
Energy Fuels 2025, 39, 4079−4093

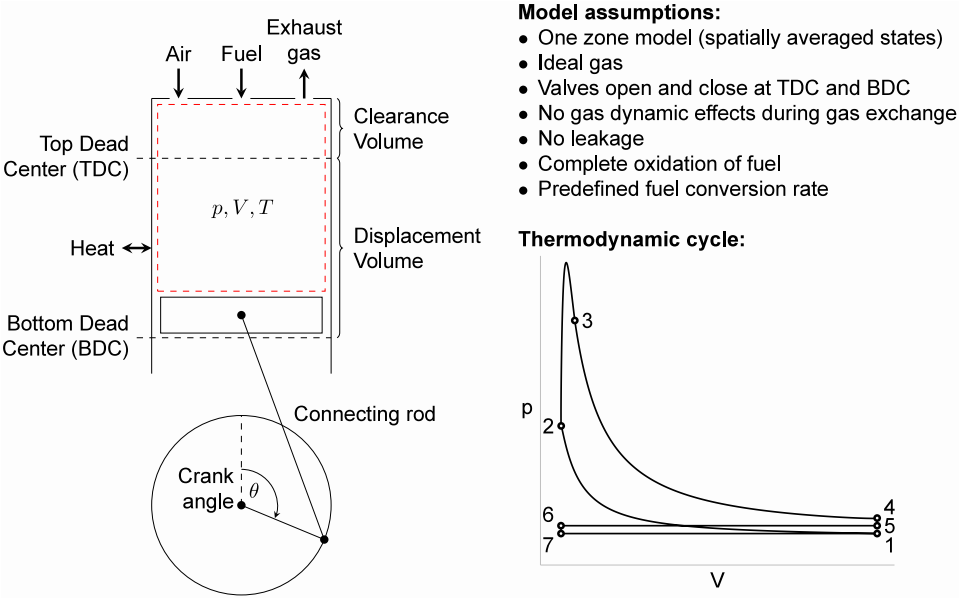

Figure 1. Left side of the figure shows a conceptual sketch of the single cylinder research engine. The piston moves between top dead center (TDC) and bottom dead center (BDC). The red box depicts the time-dependent control volume V used for the governing equations that calculate the average cylinder pressure p and the average cylinder temperature T. Mass and heat flows across the system boundary are shown. The right side illustrates the thermodynamic engine cycle on which we base the model.

THERMODYNAMIC ENGINE MODEL

Model Scope and Assumptions. The engine model shall predict the net indicated efficiency and the occurrence of knock in a single-cylinder research engine (see Figure 1, left) as a function of compression ratio, intake pressure, and fuel composition. In defining the fuel composition, we distinguish between blend stocks and components: blend stocks can refer to pure components, e.g., ethanol, or predefined mixtures, e.g., gasoline; components refer to both the pure components and the components used to model the predefined mixtures, e.g., iso-octane, toluene, or *n*-heptane, in the case of gasoline. We denote the mole fractions of blend stocks with $z_{\mathrm{fuel},j}$, and the mole fractions of components with $x_{\mathrm{fuel},j}$.

The net indicated efficiency $\eta_{\mathrm{i,n}}$ is a function of the net indicated work $W_{\mathrm{i,n}}$ and the amount of energy contained in the fuel, which depends upon the molar amount of fuel injected per cycle $n_{\mathrm{fuel,in}}$ and the lower heating value of the fuel LHV.[3]

$$\eta_{\mathrm{i,n}} = \frac{W_{\mathrm{i,n}}}{n_{\mathrm{fuel,in}}\mathrm{LHV}} \tag{1}$$

$W_{\mathrm{i,n}}$ is the area enclosed by the engine process in the pressure–volume diagram.[3]

$$W_{\mathrm{i,n}} = \oint p\,\mathrm{d}V \tag{2}$$

We base our model on the thermodynamic engine model by Gschwend et al.[55] The model by Gschwend et al. is an one-zone model, i.e., the state variables are assumed to be spatially uniform across the whole cylinder, also disregarding any differences between burned and unburned gas. Only to predict knock, the unburned gas temperature is modeled separately. Because we made different assumptions in some cases, we opted to derive the majority of model equations starting from fundamental mass and energy balances following standard assumptions.[3,50,58] Importantly, we relax Gschwend's assumption of complete exhaust of the exhaust gas, which would require a vacuum behind the exhaust valve. To this end, we introduce an idealized gas exchange model based on an idealized thermodynamic cycle with fixed valve timing, as described in Heywood[3] and in the following paragraph.

The thermodynamic cycle contains seven process steps (see Figure 1) and can be divided into a high pressure cycle and a low pressure cycle. At point 1, intake of fresh air and fuel injection are completed, and the intake valve closes instantly. Here, the high-pressure cycle begins. Between point 1 and point 2, the piston compresses the air–fuel mixture. Between point 2 and point 3, the fuel is oxidized. From point 3 to point 4, the cylinder charge expands. At point 4, the exhaust valve opens. Here, the low-pressure cycle begins. From point 4 to point 5, the pressure drops instantaneously to the pressure of the exhaust manifold. From point 5 to point 6, the piston movement purges the exhaust gas at constant pressure. At point 6, the exhaust valve closes and the intake valve opens. Between point 6 and point 7, the cylinder pressure instantaneously takes the value of the pressure in the intake manifold. Between point 7 and point 1, the piston takes in the fresh air at constant pressure and fuel is injected.

In the following, we list the most important model equations. The remaining model equations and the derivations are given in the Supporting Information. Note that the equations are expressed in terms of molar amounts instead of mass, in contrast to commonly published engine model equations.

High Pressure Cycle. The heat transfer to and from the walls is modeled with Newton's law and utilizing the Hohenberg correlation[59] for the heat transfer coefficient. The wall heat transfer term is further multiplied with an empirical heat transfer multiplier C_{HT} that can take different values for the three process steps (compression, combustion, and expansion), as commonly applied in thermodynamic engine models.[48] The values for C_{HT} are fitted to experimentally measured pressure curves.

https://doi.org/10.1021/acs.energyfuels.4c04775
Energy Fuels 2025, 39, 4079–4093

The model by Gschwend et al.[55] defines the combustion using three subsequent idealized thermodynamic processes (isochoric, isobaric, isothermal). To obtain more realistic pressure curves for the combustion phase, we replace the idealized process steps by predefining the fuel conversion rate. Specifically, we apply a Wiebe function,[60,61] which specifies the mass fraction burned ξ as a function of the crank angle θ using the parameters a, b, m, θ_0, and $\Delta\theta$.

$$\xi(\theta) = b\left\{1 - \exp\left[-a\left(\frac{\theta - \theta_0}{\Delta\theta}\right)^{(m+1)}\right]\right\} \tag{3}$$

Note that the parameters a and $\Delta\theta$ are not independent: For any combination of parameter values $\{a, m, \Delta\theta\}$, alternative combinations $\{a^*, m, \Delta\theta^*\}$ can be found so that

$$\Delta\theta^* = \left(\frac{a^*}{a}\right)^{1/(m+1)} \Delta\theta \tag{4}$$

Therefore, we set a to 1. The parameter b is not part of the original Wiebe function and was added by Yeliana et al.[61] to achieve a mass fraction burned of 1 within a finite crank angle. The choice $b = 1$ would yield the original Wiebe function where full combustion is achieved at an infinite crank angle, whereas $b > 1$ yields full combustion at finite crank angles. Our choice for a then results in the following Wiebe function with four remaining parameters:

$$\xi(\theta) = b\left\{1 - \exp\left[-\left(\frac{\theta - \theta_0}{\Delta\theta}\right)^{(m+1)}\right]\right\} \tag{5}$$

Low Pressure Cycle. For the low-pressure cycle, the pressure values are determined by intake and exhaust pressures. Further equations are needed to calculate the amount of substance in the cylinder n_1, the in-cylinder temperature T_1, and the molar amounts of air taken in $n_{\mathrm{air,in}}$, and fuel injected $n_{\mathrm{fuel,in}}$. In accordance with the idealized modeling approach, we formulate a mole balance that equals n_1 to the sum of $n_{\mathrm{air,in}}$, $n_{\mathrm{fuel,in}}$, and the molar amount of exhaust gas at state 6, n_6.

$$n_1 = n_6 + n_{\mathrm{air,in}} + n_{\mathrm{fuel,in}} \tag{6}$$

$n_{\mathrm{air,in}}$ and $n_{\mathrm{fuel,in}}$ are related through the stoichiometric coefficient of oxygen $\nu_{\mathrm{O_2}}$ and the molar fraction of oxygen in air $x_{\mathrm{O_2,air}}$.

$$n_{\mathrm{fuel,in}} = \frac{x_{\mathrm{O_2,air}}}{|\nu_{\mathrm{O_2}}|} n_{\mathrm{air,in}} \tag{7}$$

We furthermore formulate an enthalpy balance for the intake phase that equals the enthalpy of the fuel−air mixture at state 1, H_1, to the sum of the enthalpy of the exhaust gas at state 6, H_6, the enthalpy of the air taken in, $H_{\mathrm{air,in}}$, the enthalpy of the fuel injected, $H_{\mathrm{fuel,in}}$, and term for the wall heat transfer, $Q_{\mathrm{w,intake}}$.

$$H_1 = H_6 + H_{\mathrm{air,in}} + H_{\mathrm{fuel,in}} + Q_{\mathrm{w,intake}} \tag{8}$$

Together with the ideal gas law, i.e.

$$p_1 V_1 = n_1 R T_1 \tag{9}$$

which contains the known pressure p_1 and volume V_1 at the end of the intake stroke as well as the molar gas constant R, and the unknowns T_1 and n_1, $n_{\mathrm{air,in}}$ and $n_{\mathrm{fuel,in}}$ can be calculated.

The wall heat transfer term $Q_{\mathrm{w,intake}}$ accounts for the fresh air being heated up during the intake stroke, both in the intake manifold and in the cylinder. Because a higher amount of air taken in leads to a higher heat transfer from the intake manifold and the cylinder walls to the air, we assume $Q_{\mathrm{w,intake}}$ to be a function of $n_{\mathrm{air,in}}$. We furthermore consider the cooling effect of the enthalpy of vaporization of the fuel $H_{\mathrm{vap,fuel}}$ on the fuel−air mixture and the resulting increase of wall heat transfer. We assume the influence of both effects to be linear, with the parameters $C_{Q,\mathrm{air}}$ determining the influence of the amount of air taken in, and $C_{Q,\mathrm{vap}}$ determining the influence of the evaporation cooling.

$$Q_{\mathrm{w,intake}} = C_{Q,\mathrm{air}} n_{\mathrm{air,in}} + C_{Q,\mathrm{vap}} H_{\mathrm{vap,fuel}} \tag{10}$$

$H_{\mathrm{vap,fuel}}$ is the product of $n_{\mathrm{fuel,inj}}$ and the molar enthalpy of vaporization of the fuel $h_{\mathrm{vap,fuel}}$.

$$H_{\mathrm{vap,fuel}} = n_{\mathrm{fuel,in}} h_{\mathrm{vap,fuel}} \tag{11}$$

To estimate the parameters $C_{Q,\mathrm{air}}$ and $C_{Q,\mathrm{vap}}$, the term $Q_{\mathrm{w,intake}}$ is determined by using measured fuel mass flows $\dot{m}_{\mathrm{fuel}}$, as explained in the section Parameter estimation. $\dot{m}_{\mathrm{fuel}}$ is related to $n_{\mathrm{fuel,in}}$ via the rotational speed N and the molar mass of the fuel M_{fuel}.

$$\dot{m}_{\mathrm{fuel}} = \frac{n_{\mathrm{fuel,in}} M_{\mathrm{fuel}} N}{2} \tag{12}$$

For the exhaust stroke, we derive analogous mole and energy balances to calculate the molar amount and temperature of the residual gas, but pragmatically neglect the heat transfer. The equations are given in the Supporting Information.

Knock Prediction. Knock occurs when the unburned air−fuel mixture autoignites. To predict the occurrence of knock, we need to estimate the temperature of the unburned gas T^{ub} during the combustion process. For this purpose, we follow the approach of Gschwend et al.[55] who assumed identical pressure p in burned and unburned gas and no heat transfer from burned to unburned gas, reflecting typical assumptions,[50] and furthermore neglected the heat transfer from the unburned gas to the cylinder wall, as the heat transfer is calculated in the one-zone model using the temperature averaged over the whole cylinder. The temperature of the unburned zone can then be calculated with the following equation derived from the energy balance for isentropic compression of the unburned gas,[55] using the universal gas constant R and the heat capacity of the unburned gas $\bar{c}_{\mathrm{p}}^{\mathrm{ub}}$.

$$\frac{\bar{c}_{\mathrm{p}}^{\mathrm{ub}}}{R T^{\mathrm{ub}}} \frac{\mathrm{d}T^{\mathrm{ub}}}{\mathrm{d}t} = \frac{1}{p}\frac{\mathrm{d}p}{\mathrm{d}t} \tag{13}$$

Using the temperature of the unburned zone, the autoignition delay time of the unburned fuel−air mixture is calculated using the Livengood−Wu integral.[62] It yields the value k_{I} by integrating the reciprocal of the ignition delay time τ from the time at which the combustion starts, t_2, to the time combustion is completed, t_3.

$$k_{\mathrm{I}} = \int_{t_2}^{t_3} \frac{1}{\tau(p, T^{\mathrm{ub}})}\,\mathrm{d}t \tag{14}$$

https://doi.org/10.1021/acs.energyfuels.4c04775
Energy Fuels 2025, 39, 4079−4093

The ignition delay time is commonly modeled with an Arrhenius equation with the parameters A, T_A, p_{ref}, and β.

$$\tau = A \exp\left(\frac{T_A}{T}\right)\left(\frac{p}{p_{ref}}\right)^{\beta} \tag{15}$$

Douaud and Eyzat[63] proposed the values $A = 0.01869\ \mathrm{s}(\mathrm{RON}/100)^{3.4017}$, $T_A = 3800$ K, $p_{ref} = 1 \times 10^5$ Pa, and $\beta = 1.7$ for gasoline fuels. However, alternative fuels may exhibit different autoignition behavior that is not adequately captured by the RON. Therefore, we parametrize Arrhenius models for every blend component using kinetic ignition delay simulation data. For fuels that exhibit two-stage autoignition behavior, we use the 3-Arrhenius approach[64] that models the ignition delay as a function of three ignition delay times τ_1, τ_2, and τ_3 for low, medium, and high temperature regimes, respectively:

$$\frac{1}{\tau} = \frac{1}{\tau_1 + \tau_2} + \frac{1}{\tau_3} \tag{16}$$

The ignition delay times for the specific regimes are each modeled with an Arrhenius equation. Details on kinetic mechanisms, software, simulated conditions, and fitting are listed in the Supporting Information. Ignition delay times of fuel blends can be subject to nonlinear mixing rules, depending upon kinetic interactions between the blend constituents and their combustion intermediates. However, dedicated rigorous kinetic models are not available for most blend stock combinations. The mixture behavior can be idealized by applying a linear-by-mole mixing rule to the logarithm of the ignition delay time, as can be observed, e.g., for a mixture of dimethyl ether and *n*-pentane.[65] For blend stocks that are predefined mixtures, such as gasoline, kinetic models are available. Hence, we calculate the ignition delay of a fuel blend as a function the mole fractions of the blend stocks j, $z_{\mathrm{fuel},j}$, summing over the set of possible blend stock $N_{\mathrm{blend\ stocks}}$.

$$\ln \tau = \sum_{j \in N_{\mathrm{blend\ stocks}}} z_{\mathrm{fuel},j} \ln \tau_j \tag{17}$$

Parameter Estimation. Several parameters of the engine model must be estimated from experimental data: the heat transfer multipliers $C_{\mathrm{HT,Compr}}$, $C_{\mathrm{HT,Comb}}$, and $C_{\mathrm{HT,Expan}}$, the parameters b, θ_0, $\Delta\theta$, and m of the Wiebe function (see eq 5), and the parameters $C_{Q,\mathrm{air}}$ and $C_{Q,\mathrm{vap}}$ from the correlation that models the heat transfer during intake (see eq 10). We use measurement data obtained with a single-cylinder research engine with a compression ratio of 16.4 described previously[16] and perform regression using numerical optimization. Table 1 lists the most important specifications of the experimental engine. We estimate all model parameters using measurement series of load variation for the alternative fuels ethanol and 2-butanone under stoichiometric combustion conditions at a rotational speed of 2000 min^{-1}. Subsequently, we validate the model with measurement series of the alternative fuel KEAA[16,32] and conventional RON 95 E10 gasoline.

Table 1. Specifications of the Single-Cylinder Research Engine[16]

parameter	value
displacement volume (cm^3)	500
bore (mm)	75
stroke (mm)	113.2
connecting rod length (mm)	220
compression ratio	16.4

First, the heat transfer multipliers and the Wiebe function parameters are fitted to the pressure curve for each load point separately. We discard load points with knock limitation, i.e., points from the ethanol measurement series at intake pressure higher than 1.5 bar.[16] During parameter estimation, the intake stroke is calculated in a different manner than described in the previous section: We calculate $n_{\mathrm{fuel,in}}$ from the fuel mass flow measured in the experiment. Then, we determine $n_{\mathrm{air,in}}$ using eq 7 and n_1 using eq 6. T_1 is then calculated using the ideal gas law, and the enthalpy H_1 is calculated using the molar amounts and T_1. The wall heat transfer term $Q^*_{\mathrm{w,intake}}$ is then calculated in the following manner:

$$Q^*_{\mathrm{w,intake}} = H_1 - H_6 - H_{\mathrm{air,in}} - H_{\mathrm{fuel,in}} \tag{18}$$

The heat transfer multipliers and the Wiebe function parameters are fitted to minimize the absolute root mean squared error of the simulated pressure $p(\theta_i)$ with regard to the pressure measurements $\tilde{p}(\theta_i)$ from $\theta_i = -175°$ to $\theta_i = 175°$, where i is index for the measurement samples. Data for crank angles between $\theta_i = -180°$ (BDC) to $\theta_i = -175°$ are discarded because the experimental pressure curve is affected by the valve closing right after BDC. Equally, data for crank angles between 175° (BDC) and 180° are discarded because the experimental pressure curve is affected by the valve opening right before BDC. In summary, we minimize the least-squares error for every load point.

$$\min_{b,\theta_0,\Delta\theta,m,C_{\mathrm{HT,Compr}},C_{\mathrm{HT,Comb}},C_{\mathrm{HT,Expan}}} \sum_i (p(\theta_i) - \tilde{p}(\theta_i))^2 \ \forall$$
$$\theta_i \in \{-175°, 175°\} \tag{19}$$

Parameter estimation of dynamic nonlinear models can often lead to suboptimal fits due to non-convexity.[66] To avoid this, we use the MATLAB[57] multistart optimization solver Global Search with fmincon as a local optimization solver. We provide bounds for every parameter (see Table 2). The heat transfer multipliers being correction factors to a semi-empirical heat

Table 2. Generalized Parameter Values of Thermodynamic Engine Model[a]

parameter	lower bound	upper bound	value
heat transfer mulitplier			
$C_{\mathrm{HT,Compr}}$	0.1	10	3.2
$C_{\mathrm{HT,Comb}}$	0.1	10	6.2
$C_{\mathrm{HT,Expan}}$	0.1	10	0.1
switching point for heat transfer mulitplier			
$\xi_{\mathrm{HT,Expan},0}$			1
$\delta_{\mathrm{HT,Expan}}$			−0.03
Wiebe function			
b	1	1.1	1.04
θ_0 (deg)	−11	0	−2.5
$\Delta\theta$ (deg)	9	22	13.7
m	0.3	2.6	1.1
heat transfer during intake			
$C_{Q,\mathrm{vap}}$	0	1	0.65
$C_{Q,\mathrm{air}}$ ($\mathrm{J\ mol}^{-1}$)	0	2000	920

[a]Note: For the heat transfer multipliers and the Wiebe function paramerters, the lower and upper bounds have been used during the load point- and fuel-specific parameter estimation.

https://doi.org/10.1021/acs.energyfuels.4c04775
Energy Fuels 2025, 39, 4079−4093

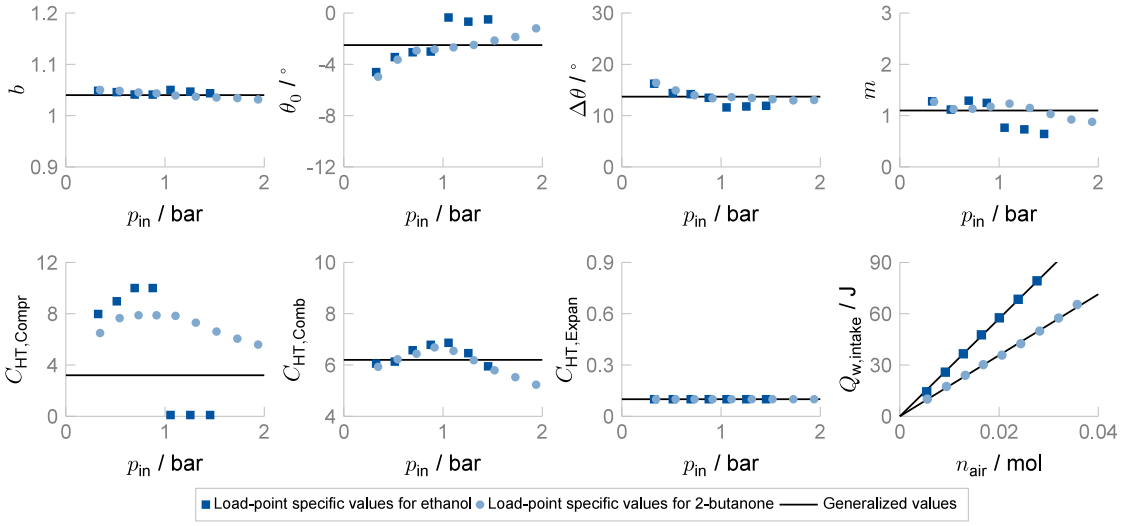

Figure 2. Parameters b, θ_0, $\Delta\theta$, m, $C_{HT,Compr}$, $C_{HT,Comb}$, and $C_{HT,Expan}$ for individual load points and fuels (denoted with blue markers) as well as the averaged values, i.e., the deduced generalized parameter values (denoted with black lines). For $C_{HT,Compr}$, the generalized parameter value is not obtained by averaging, but by performing a sensitivity analysis of the knock calculation, resulting in a parameter value smaller than the average of the load-point specific parameters. For the term $Q_{w,intake}$, the black lines denote the values obtained with the load- and fuel-specific correlation (10) for ethanol and 2-butanone.

transfer correlation are constrained to the interval [0.1, ..., 10]. The derivation of bounds for the Wiebe function parameters are explained in section 3 of the Supporting Information.

The load-point specific parameters resulting from the parameter estimation are plotted in Figure 2. To derive load-independent parameters, we take the arithmetic average of the load-point specific values for b, θ_0, $\Delta\theta$, m, $C_{HT,Comb}$, and $C_{HT,Expan}$. For $C_{HT,Compr}$, we make an exception, as the values fitted to the pressure curves of ethanol alternate between very high and very low values, reaching either the lower or the upper bound for most load points. Apparently, the optimizer tries to compensate for a structural model error by setting $C_{HT,Compr}$ to either a very high or very low value. Instead of taking the average of the load-point specific values, we use $C_{HT,Compr}$ to fine-tune the prediction of knock, following Vancoillie et al.[48] To this end, we perform a sensitivity analysis of $C_{HT,Compr}$ with respect to the knock prediction for the highest load point of 2-butanone (which is not knock limited in the experiment) and the second and third highest load points of ethanol (one of which is knock limited, whereas the other one is not). The first plot in Figure 3 shows the values of the Livengood–Wu integral for the three selected load points with varying $C_{HT,Compr}$. It shows that knock is overestimated for the highest load point of 2-butanone for $C_{HT,Compr} < 2.9$ and knock is underestimated for the second highest load point of ethanol for $C_{HT,Compr} > 3.6$. Hence, $C_{HT,Compr}$ should lie between 2.9 and 3.6 and we choose $C_{HT,Compr} = 3.2$.

Furthermore, we note that all values for $C_{HT,Expan}$ are located at the lower bound. A closer inspection suggests that the optimizer tries to compensate for a structural model error by setting $C_{HT,Expan}$ as low as possible. Specifically, a variation of $C_{HT,Expan}$ shows that the root mean squared error monotonously decreases with decreasing $C_{HT,Expan}$ (see lower plot in Figure 3). Further clues can be derived from a comparison of the pressure curves of the experiment and the model. Figure 4 (top) shows the pressure curves for an exemplary load point of 2-butanone. Although, in general, the simulated pressure curve (dashed line) matches the experimentally measured pressure curve (solid line) well, the pressure during the expansion is

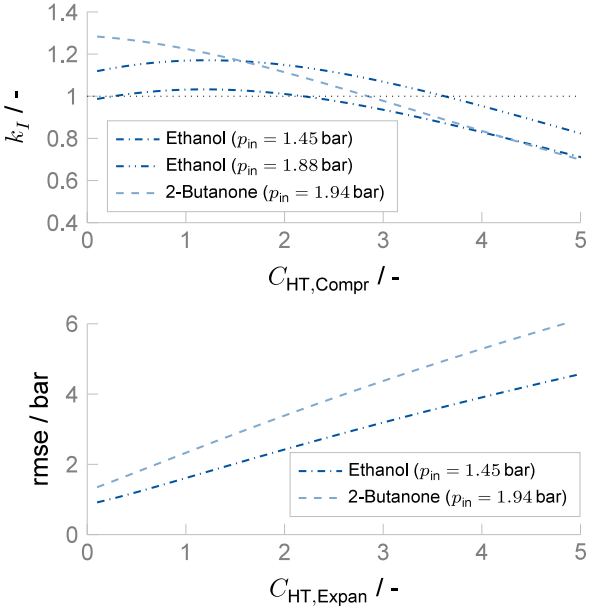

Figure 3. Sensitivity of knock index k_I with respect to the heat transfer multiplier during compression $C_{HT,Compr}$ (top) and influence of the heat transfer multiplier during expansion $C_{HT,Expan}$ on the root mean squared error (rmse) of the pressure curve during expansion (bottom).

underestimated, which can be partly compensated for with a low value for $C_{HT,Expan}$. To illustrate the effect on the calculated net indicated work, we calculate the cumulative net indicated work as a function of θ (Figure 4, center).

$$W_{i,n}(\theta) = \int_{V(\theta_0)}^{V(\theta)} p(\tilde{\theta})\mathrm{d}V(\tilde{\theta}) \tag{20}$$

Whereas initially the cumulative net indicated work of the experiment is matched very well, a deviation becomes evident for the expansion stroke after the combustion. Here, the pressure is underestimated an thus the net indicated work is

https://doi.org/10.1021/acs.energyfuels.4c04775
Energy Fuels 2025, 39, 4079−4093

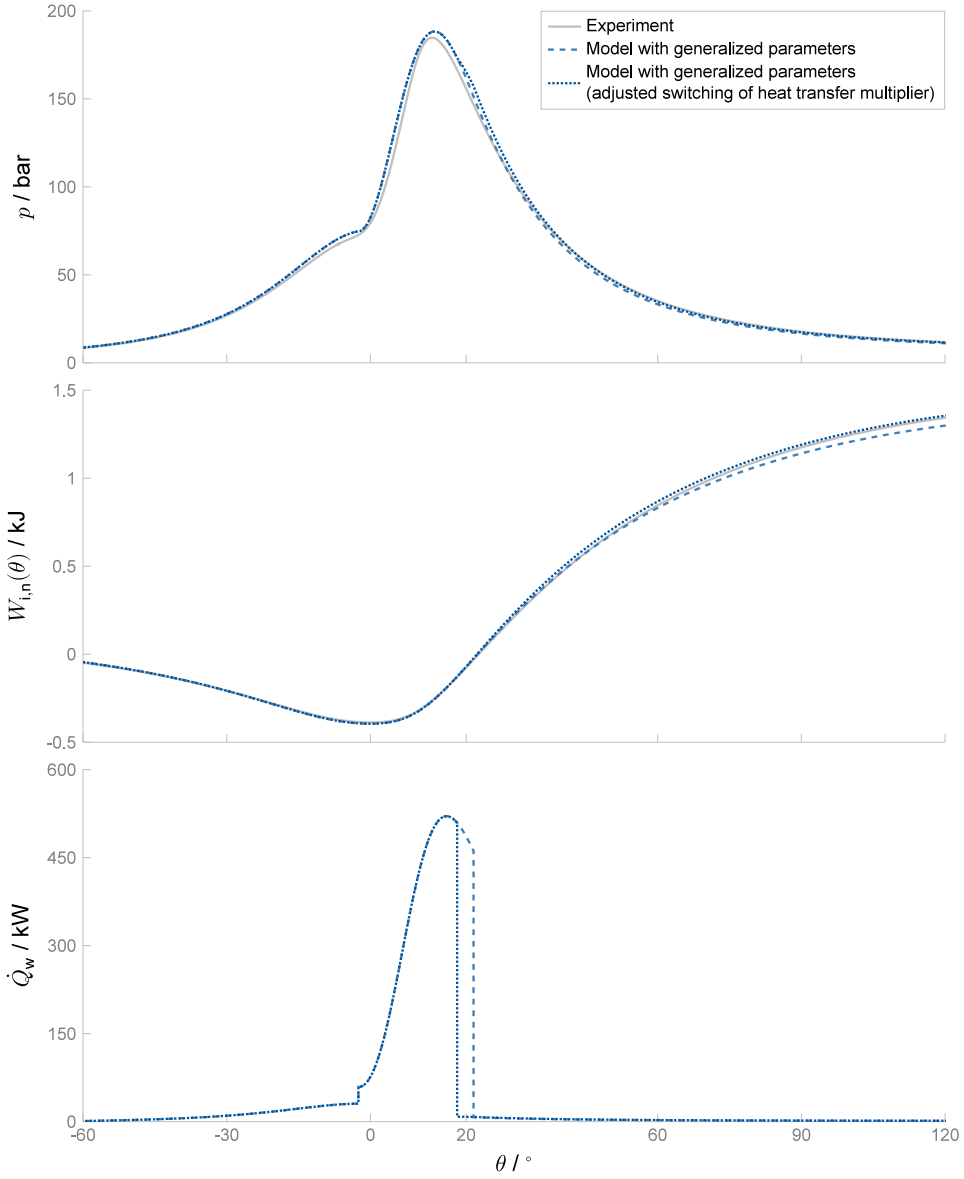

Figure 4. Experimental and simulated pressure curve (top) and cumulative net indicated work curve (center) during the high pressure cycle for 2-butanone at intake pressure 1.94 bar, as well as simulated heat transfer (bottom). For the simulated values, the dashed lines denote the curves for the model using the generalized parameters before correcting the switching point of the heat transfer multipliers $C_{HT,Comb}$ and $C_{HT,Expan}$, whereas the dotted line denotes the curves for the correction achieved with eq 22.

underestimated. This effect is reduced by choosing the lowest possible value for $C_{HT,Expan}$.

A plot of the heat transfer over the crank angle (cf. Figure 4, bottom) shows very high values for the heat transfer during combustion and a discrete change to very low values when the combustion is finished. The discontinuity is caused by the discrete switch in the piece-wise constant heat transfer multipliers. The piece-wise definition of heat transfer multipliers allows for a convenient calibration of the pressure curves to experimental data, but it oversimplifies the physical processes in the cylinder. $C_{HT,Comb}$ exhibits a high value to match the experimental pressure peak. However, with the switching point to a lower value being determined by the Wiebe function parameters, the heat transfer during later phases of the combustion appears to be overestimated. Selecting a small value for $C_{HT,Expan}$ is not enough to compensate for the late switching.

To implement a pragmatic correction of the underestimation of the work, we modify the model by including an adjustable switching point. To that end, we introduce a new parameter $\xi_{HT,Expan}$ that determines the degree of fuel conversion at which the heat transfer multiplier is switched. First, we fit the value of $\xi_{HT,Expan}$ directly to the experimental values of the net indicated efficiency $\tilde{\eta}_{i,n}$ for every load point, i.e., we solve

$$\min_{\xi_{HT,Expan}} (\eta_{i,n} - \tilde{\eta}_{i,n})^2 \tag{21}$$

The load-point specific switching points are plotted in Figure 5. We observe an approximately linear correlation between intake pressure and the optimal switching point, resulting in the following relation for determining $\xi_{HT,Expan}$:

$$\xi_{HT,Expan} = \xi_{HT,Expan,0} + \delta_{HT,Expan}\left(\frac{p_{in}}{1\ \text{bar}}\right) \tag{22}$$

https://doi.org/10.1021/acs.energyfuels.4c04775
Energy Fuels 2025, 39, 4079−4093

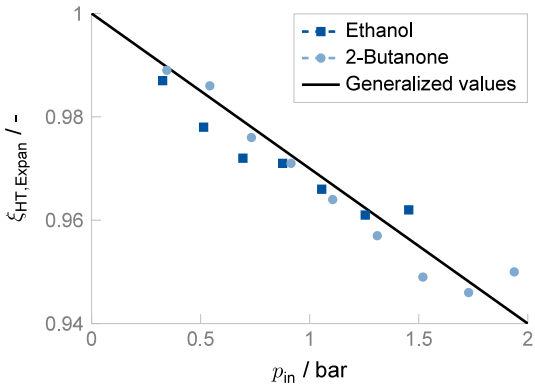

Figure 5. Optimal switching points $\xi_{HT,Expan}$ for switching the heat transfer multiplier of combustion to the heat transfer multiplier of expansion. The markers denote the values obtained by fitting the net indicated efficiency of every load point. The line denotes the derived general linear correlation (see eq 22).

The resulting pressure and cumulative pressure curve for one exemplary load point are plotted in Figure 4 (dotted lines). Note that the prediction of the indicated work is corrected without altering the pressure curve peak.

Finally, the parameters $C_{Q,air}$ and $C_{Q,vap}$ are determined by minimizing the root mean squared deviation of the values of $Q^*_{w,intake}$ and $Q_{w,intake}$, i.e., the values obtained during the estimation of load-point specific parameter and the values obtained with eq 10.

$$\min_{C_{Q,air},C_{Q,vap}} \sum_i (C_{Q,air} n_{air,in,i} + C_{Q,vap} H_{vap,i} - Q^*_{w,intake,i})^2 \tag{23}$$

The lower right plot in Figure 2 shows that the linear correlation reproduces very well the values obtained for the load-point specific simulations. The full set of the resulting model parameters is listed in Table 2.

Validation. To validate the model, we compare the simulations against experimental data from our previous study[16] on the fuels ethanol, 2-butanone, KEAA, and RON 95 E10, as shown in Figure 6 (left plot). The overall trends are very well reproduced by the model: ethanol has the highest efficiency, KEAA and 2-butanone perform similarly, and RON 95 E10 exhibits the lowest efficiency.

To evaluate the quality of the knock prediction, we compare the intake pressure at which knock begins to occur in the model with the intake pressure, at which the efficiencies measured in the experiment decrease as a consequence of spark retardation due to a knock limitation. For the model prediction, we examine the values for the Livengood–Wu integral k_I, using both the Douaud–Eyzat model[63] and a kinetics-based model for each fuel. In Figure 7, the values for k_I are plotted over the intake pressure in one plot for each fuel, and the areas that correspond to over- or underestimation of knock are colored. The plots show that the Douaud–Eyzat model only predicts knock of RON 95 E10 gasoline well. For the alternative fuels, the Douaud–Eyzat model overestimates the autoignition with increasing intake pressures, leading to severe overestimation of knock already at throttled conditions.

In contrast, the kinetics-based ignition delay model predicts knock qualitatively well. However, we observe errors for the fuels that have not been used in the calibration of the model. For KEAA, the model incorrectly predicts the absence of knock, wheres in the experiment intake pressures greater than 1.7 bar lead to knock. Here, k_I reaches a value of 0.83, which is a significant but not severe deviation from a value greater than 1. The underestimation of knock might be caused by the exclusion of nonlinear blending effects in the ignition delay time (see eq 17). Another factor could be the simplified fuel evaporation model that might lead to inaccurate in-cylinder temperatures. For RON 95 E10, the occurrence of knock is slightly overestimated: the model predicts knock already at intake pressures of 0.5 bar, whereas in the experiment, a knock limitation is observed at intake pressures higher than 0.6 bar. Unsurprisingly, the calculation of knock is correct for ethanol and 2-butanone, as data on these fuels have been used for the calibration of the model. In summary, we consider the kinetics-based models a significant improvement over the Douaud–Eyzat model for the alternative fuels.

To validate the engine model for different compression ratios, we compare its predictions with experimental data from Wouters et al.[19] using methanol as a fuel at compression ratios of 10.8 and 17.7, as well as previously unpublished data using ethanol at a compression ratio of 17.7 in the same engine (see

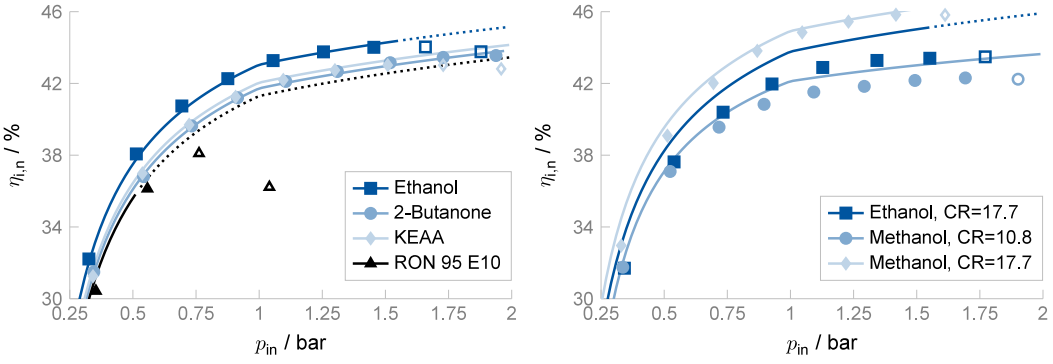

Figure 6. Efficiency calculation: the left plot shows net indicated efficiencies at varied intake pressures for RON 95 E10, ethanol, 2-butanone, and KEAA, using single-cylinder research engine data from Ackermann et al.;[16] the right plot shows indicated efficiencies for methanol with compression ratios (CRs) of 10.8 and 17.7 using single-cylinder research engine data from Wouters et al.[19] as well as previously unpublished data for ethanol with CR 17.7, measured in the same engine. Note that for the right plot, the engine runs at a rotational speed of 2500 min^{-1}, which differs from the rotational speed of 2000 min^{-1} used in the measurements shown in the other plots. The markers denote the measurement values. Nonfilled markers indicate that the ignition has been retarded due to knock limitation. The lines denote the simulation results. Dotted lines indicate the occurrence of knock.

https://doi.org/10.1021/acs.energyfuels.4c04775
Energy Fuels 2025, 39, 4079–4093

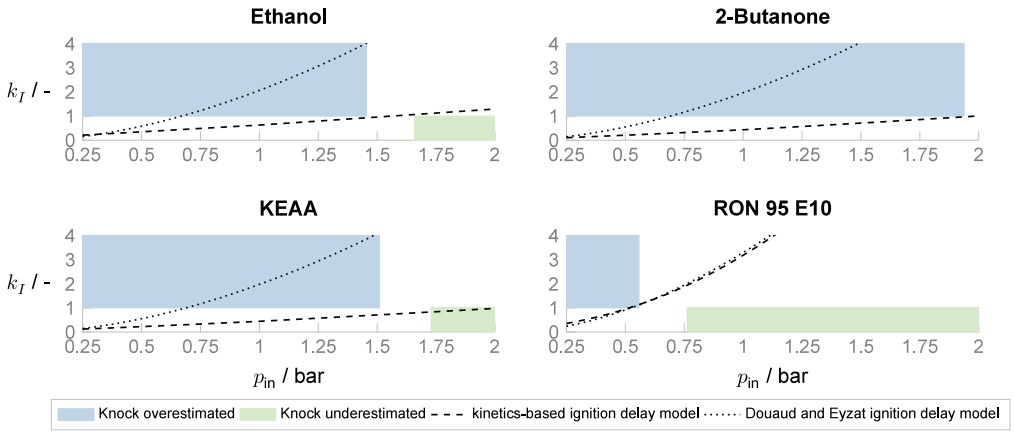

Figure 7. Knock calculation: The value of the Livengood–Wu integral k_I is plotted over the intake pressure for the fuels ethanol (top left), 2-butanone (top right), KEAA[16,32] (bottom left), and RON 95 E10 (bottom right). Blue areas denote the regions where knock is overestimated, green areas denote the regions where knock is underestimated. Dotted lines denote the values for k_I calculated with the ignition delay model by Douaud and Eyzat[63] (15), dashed lines denote the values for k_I calculated with Arrhenius ignition delay models fitted to data from zero-dimensional kinetic simulations under isochoric conditions.

Figure 6, right plot) at a rotational speed of 2500 min^{-1}, which differs from the rotational speed of 2000 min^{-1} in the experiments used of the fitting. Furthermore, the combustion is phased differently, leading to burn profiles different from those used in the parameter estimation. Hence, we compare the data in qualitative terms. The general trends are replicated well: a higher compression ratio leads to higher indicated efficiencies, and methanol yields a higher efficiency than ethanol at the same compression ratio. At the low compression ratio, the model does not predict knock for methanol at high loads where knock is observed in the experiment. At the high compression ratio, the model slightly overpredicts knock for ethanol.

We conclude that the engine model predicts trends in net indicated efficiency and the onset of knock reasonably well for fuels and compression ratios that were not used in the fitting. However, as we lack more validation data for a comprehensive judgment of the model performance, in particular regarding the onset of knock, the fuels designed using the engine model must be experimentally validated.

CO-OPTIMIZATION OF FUEL BLEND AND ENGINE

Problem Formulation. We maximize the net indicated efficiency $\eta_{i,n}$ as a function of the compression ratio ε_{CR}, the intake pressure p_{in}, and the vector of molar blend stock compositions $\boldsymbol{z}$, whose size depends upon the number of possible blend stocks. For the engine, we consider the parameters of our single-cylinder research engine (see Table 1) and fix the rotational speed to 2000 min^{-1}. Following Gschwend et al.,[55] we allow for compression ratios between 5 and 20, constrain the value of the Livengood–Wu integral k_I to less than or equal to 0.99 to avoid knock. The peak pressure p_{peak} is constrained to less than or equal to the limit of our single-cylinder research engine, i.e., 200 bar.[19] Moreover, we optimize the intake pressure, covering the range from fully opened throttle in naturally aspirated operation (1 bar) to highly boosted engine operation (2 bar).

The fuel composition is constrained by fuel specifications added to tailor the volatility of the fuel. An upper bound on the volatility is set to ensure safe handling and avoid cavitation in the fuel pump system.[67] At the same time, the fuel needs to exhibit a sufficient front-end volatility, which is crucial for in-cylinder mixture formation and thus driveability under cold conditions.[67] We tailor the volatility by imposing limits on the vapor pressure and the enthalpy of vaporization, following previous studies.[31,32] Specifically, we use the bubble point pressure p_{bubble} as an approximation for the Reid vapor pressure, as in previous fuel blend design studies,[31,32,68] and constrain it to the range [35 kPa, 100 kPa], following gasoline standards[8,9] and previous CAPD studies.[31,32,68] The enthalpy of vaporization is constrained to a value less than or equal to 60 kJ/kg_{air}, again following previous CAPD studies.[30−32,43] Because a high enthalpy of vaporization has a positive influence on engine efficiency due to charge cooling,[38] the constraint potentially limits the maximum efficiency of the designed fuel.

The overall co-optimization problem reads

$$\max_{\varepsilon_{CR}\in[5,20],p_{in}\in[1,2]\text{bar},\boldsymbol{z}\in[0,1]^{N_{\text{blend stocks}}}} \eta_{i,n}(\varepsilon_{CR}, p_{in}, \boldsymbol{z})$$

$$\text{s.t.}\quad p_{peak}(\varepsilon_{CR}, p_{in}, \boldsymbol{z}) \le 200\ \text{bar}$$

$$k_I(\varepsilon_{CR}, p_{in}, \boldsymbol{z}) \le 0.99$$

$$p_{bubble}(\boldsymbol{z}) \ge 35\ \text{kPa}$$

$$p_{bubble}(\boldsymbol{z}) \le 100\ \text{kPa}$$

$$h_{vap}(\boldsymbol{z}) \le 60\ \text{kJ/kg}_{air}$$

$$\sum_{i\in N_{\text{blend stocks}}} z_i = 1$$

where $\eta_{i,n}(\varepsilon_{CR},p_{in},\boldsymbol{z})$, $p_{peak}(\varepsilon_{CR},p_{in},\boldsymbol{z})$, and $k_I(\varepsilon_{CR},p_{in},\boldsymbol{z})$ are obtained via integrating the engine model equations, and $p_{bubble}(\boldsymbol{z})$ and $h_{vap}(\boldsymbol{z})$ are obtained via mixing rules described in the Supporting Information. We first optimize the blend composition $\boldsymbol{z}$ without the objective function and starting from an equimolar mixture using the MATLAB[57] local optimization solver fmincon. If no feasible mixture is found, the blend stock system is discarded. If a feasible mixture is found, it is used to initialize the blend composition in the co-optimization.

The problem is nonlinear and potentially contains more than one local optimum. While we expect the net indicated efficiency to increase monotonically with compression ratio and intake pressure, no such statements can be made for the fuel composition, given the nonlinear property relations. Therefore, we use the MATLAB multistart optimization solver

https://doi.org/10.1021/acs.energyfuels.4c04775
Energy Fuels 2025, 39, 4079−4093

Global Search with fmincon as a local optimization solver and set the maximum time to 2000 s. Because we do not provide analytical expressions for the derivatives, fmincon approximates the derivatives with finite differences. Note that dynamic models can be optimized more efficiently using dynamic optimization solvers.[69−71] For historical reasons, however, our model and optimization was implemented in MATLAB and we refrain from reimplemenation. We furthermore note that the degrees of freedom can be reduced by 1 by calculating the mole fraction of one component directly using the closure condition, which might be beneficial for some solvers.

We select blend stocks based on our previous CAPD studies for ultrahigh efficiency engines,[31,77] where fuel blends were optimized with respect to production process performance. The selected blend stocks are listed in Table 3. Allowing 10 possible blend stocks, the problem has 12 degrees of freedom. However, a blend containing all 10 blend stocks is unlikely to emerge and probably undesirable as it would require a complex production process. Instead, we restrict our attention to binary and ternary blends and enumerate possible blend stock combinations.

To reduce the number of blends to be optimized, we categorize the blend stocks into low reactivity blend stocks and volatility enhancing blend stocks. Table 3 shows that 6 of the 10 blend stocks lead to expected net indicated engine efficiencies between 43.7 and 45.8% (assuming a use as a pure-component fuel), whereas the other 4 blend stocks are interesting because of their volatility. Consequently, we refer to the former blend stocks as low reactivity blend stocks and the latter blend stocks as volatility enhancers. Only allowing one volatility enhancing blend stock per blend, we obtain 39 possible binary systems and 60 possible ternary systems. Every possible binary and ternary blend stock system is then co-optimized together with the engine using the above-described procedure.

Table 3. Blend Constituents with Boiling Point T_{boil}, Bubble Point Pressure p_{bubble} at 37.8 °C, Enthalpy of Vaporization h_{vap} at 25 °C, and Maximum Achievable Engine Efficiency $\eta_{i,n,max}$[a]

blend stock	RON	OS	T_{boil} (°C)	h_{vap} at 25°C (kJ/kg$_{air}$)	p_{bubble} at 37.8 °C (kPa)	$\eta_{i,n,max}$ (%)
low reactivity blend stocks						
methanol	110[74]	2[74]	65	181	32	45.8
methyl acetate	120[27]	0[27]	57	67	49	44.8
ethyl acetate	118[27]	−2[27]	77	52	23	44.6
ethanol	109[75]	19[75]	78	103	16	44.5
methyl isopropyl ketone	109[27]	7[27]	94	38	12	43.9
2-butanone	111[27]	6[27]	80	46	22	43.7
volatility enhancers						
cyclopentane	101[76]	16[76]	49	27	68	40.7
gasoline	96[76]	7[76]		25	59	38.9
n-pentane	62[76]	−1[76]	36	24	108	
n-hexane	25[76]	−1[76]	69	24	34	

[a]*n*-Pentane and *n*-hexane are no feasible pure-component fuels in the engine model due to their high auto-ignition propensity, hence, no value for $\eta_{i,n,max}$ is given. Thermophysical properties are taken from the DIPPR database,[72] the sources for RON and OS are indicated in the table. For gasoline, we use a surrogate.[73] The molar composition of the gasoline surrgate and the mixing rules for h_{vap} and p_{bubble} are given in the Supporting Information; for RON and OS we use linear-by-mole mixing rules.

Resulting Blends and Engine Configurations. The co-optimization yields 23 binary blends and 67 ternary blends. Figure 8 shows an analysis of the top-rated binary blends. It can be noted that 7 of the 8 best-performing blends contain over 50 mol % of methyl acetate and a large fraction of ethyl acetate (41 mol %, blend 1) or a ketone (33−37 mol %, blends 4 and 7) or a small fraction of a volatility enhancer (7−13 mol %, blends 2, 3, 5, and 6). These methyl acetate blends achieve predicted net indicated efficiencies from 44.5 to 44.7%. Considering the model uncertainties, they can be considered equally good. The efficiencies are achieved exploiting the maximum compression ratio of 20 and intake pressures of 1.8 bar. In all cases, the intake pressure is limited by the maximum peak pressure, not by the occurrence of knock. Moreover, all methyl acetate blends exhibit the maximum enthalpy of vaporization of 60 kJ/kg$_{air}$.

Only three blends (blends 6, 9, and 10) compete with the methyl acetate blends. They consist of a large ethyl acetate fraction (85 to 95 mol %) and a small fraction of pentane, cyclopentane, or gasoline. They achieve net indicated efficiencies of 44.1 to 44.5%, reaching compression ratios between 16.8 and 19.7 and an intake pressures of 1.8 to 2.0 bar. They are both knock and peak pressure limited.

After the top 10 blends, the next candidates utilize a ketone as the main blend stock, with small fractions of cyclopentane, pentane, or gasoline as volatility enhancers. The achieved efficiencies vary with the main blend stock: 43.2−43.4% (2-butanone), and 42.7−43.2% (methyl isopropyl ketone), and compression ratios range between 13.8 and 15.6, with the maximum intake pressure of 2 bar. All of these blends are limited by knock but not by peak pressure. The bubble point pressure always exhibits the minimum allowed value. A binary blend of 2-butanone with *n*-hexane achieves a lower efficiency.

Further blends contain ethanol or methanol as a main blend stock with gasoline, cyclopentane, or hexane as a second blend stock. The alcohol blends with cyclopentane or gasoline achieve efficiencies of 41.0 to 42.1%, the alcohol blends with hexane achieve efficiencies below 40.0%. All alcohol-based blends contain a larger volatility enhancing fraction (27−43 mol %) than the ester and ketone-based blends. All nonmethyl-acetate blends are knock limited and do not achieve the maximum compression ratio.

All blends touch a volatility constraint. The blends containing ethyl acetate, 2-butanone, or MIPK use methyl acetate or a volatility enhancer to balance their unfavorably low bubble point pressure. The blends containing methyl acetate, methanol, and ethanol require other blend stocks to balance their unfavorably high enthalpy of vaporization. Considering the charge cooling effect of the light alcohols, the chosen limit for the enthalpy of vaporization might limit the maximum achievable efficiency. Indeed, if we increase the upper limit on the enthalpy of vaporization to 80 kJ/kg$_{air}$, the two best blends contain methyl acetate and either methanol or ethanol. Both blends are predicted to achieve an efficiency of 44.9% with an enthalpy of vaporization of 80 kJ/kg$_{air}$. The third best fuel would be pure methyl acetate achieving an efficiency of 44.8%.

Interestingly, the ternary blends do not enable higher engine efficiencies than the binary blends. Two ternary blends containing methyl acetate and ethyl acetate with a small share of either methanol or ethanol can compete with the best binary blends. A graphical analysis of the top 25 ternary blends,

https://doi.org/10.1021/acs.energyfuels.4c04775
Energy Fuels 2025, 39, 4079−4093

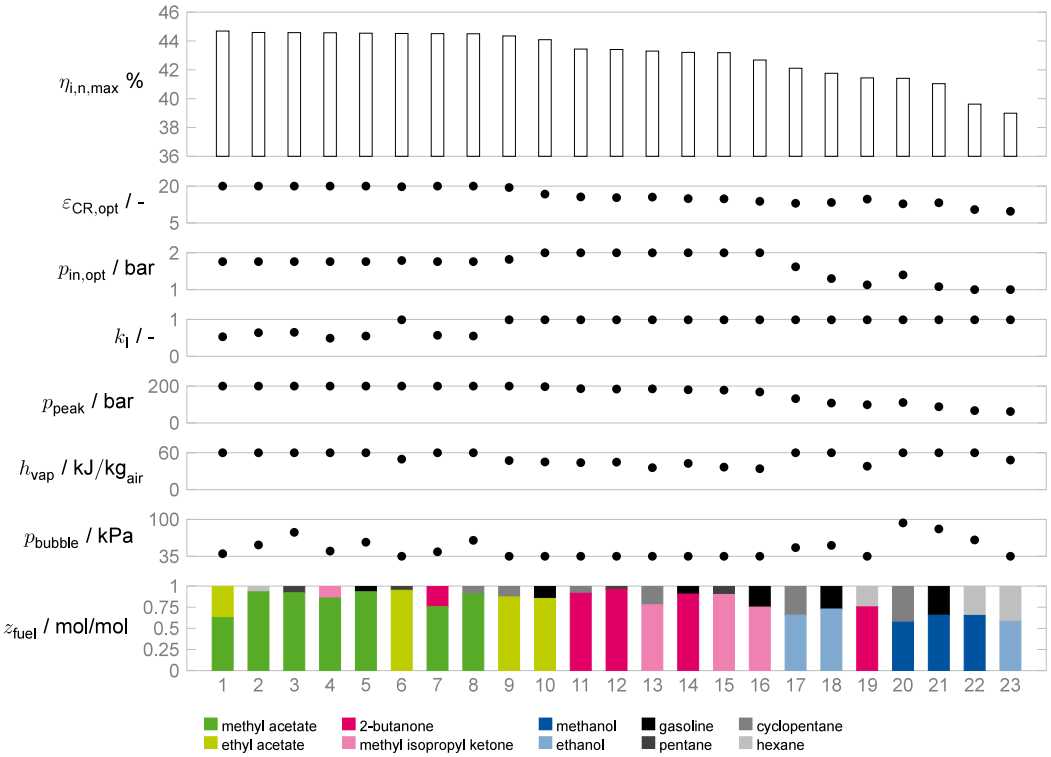

Figure 8. Binary blends resulting from the co-optimization. We sort the blends by their achievable net indicated efficiency $\eta_{i,n,max}$ (plotted at the top). We furthermore plot engine design and operation variables and the fuel properties in relation to their upper and lower bounds: the optimal compression ratio $\varepsilon_{CR,opt}$, the optimal intake pressure $p_{in,opt}$, the resulting value of the Livengood–Wu integral k_I as a measure for knock, the resulting peak pressure p_{peak}, the enthalpy of vaporization h_{vap}, the bubble point pressure p_{bubble}, and the molar composition z_{fuel}.

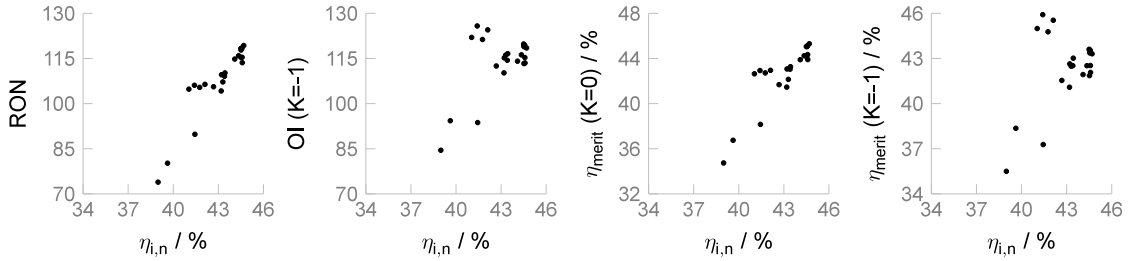

Figure 9. Comparison of the engine efficiency predicted by our model with RON (left), OI[11] (center-left), and merit function[2] (center-right and right) for all binary blends. Research and motor octane numbers of the blends were calculated using the linear-by-mole mixing rule. For the gasoline-containing blends, the efficiency values calculated with the engine efficiency merit function are obtained with the gasoline surrogate[73] used throughout this study.

similar to the one for the binary blends (Figure 8), can be found in Figure S1 of the Supporting Information.

The co-optimization thus reveals small esters as the most promising blend stocks, outperforming the ketone and alcohol blends. Several studies have pointed out the octane boosting qualities of methyl and ethyl acetate.[27,32,78] In a previous molecular design study,[43] we also identified small esters as potential fuel candidates to maximize SI engine efficiency, but pointed to their low octane sensitivities and low laminar burning velocities as potential drawbacks. A presumable influence of the laminar burning velocity is ignored by the engine model, as the burning progress is equal for all fuels. Thus it is conceivable that the engine model overestimates the efficiencies for small esters. The octane sensitivity, however, is a measure for the influence of engine conditions on knock. Our model simulates the engine conditions and predicts the occurrence of knock using ignition delay surrogate models that rely on detailed kinetic mechanisms. Leppard[12] links low octane sensitivity with low-temperature heat release observed in alkane combustion. However, methyl acetate and ethyl acetate do not exhibit low-temperature heat release.[79] It is therefore questionable whether octane sensitivity is a useful measure for the knock resistance of small esters.

The engine model predicts methyl acetate blends to be limited by the peak pressure restriction, not by the occurrence of knock. This is an interesting finding because, in our previous experimental investigations, even highly knock-resistant fuels exhibited knock under extreme conditions, e.g., methanol in an engine with a compression ratio of 17.7.[19] Assuming the absence of knock is predicted correctly, the use of stronger engine materials could facilitate higher peak pressures and thus even higher efficiencies of methyl acetate blends. In general, the material compatibility of small esters needs to be

https://doi.org/10.1021/acs.energyfuels.4c04775
Energy Fuels 2025, 39, 4079−4093

investigated, in order to assess weather they are suitable for engines and fuel systems.

Several top blends do not require a volatility enhancer. Instead, they balance the volatility related properties of the low-reactivity blend stocks; i.e., they combine the high vapor pressure of methyl acetate with the low enthalpy of vaporization of ethyl acetate or a ketone. For blends that do contain volatility enhancers, the co-optimization favors gasoline, pentane, and cyclopentane over *n*-hexane.

Cyclopentane and gasoline are predicted to not impede too strongly the knock resistance of a blend under rather extreme engine conditions. It shall be noted though that the linear-by-mole mixing rule for the ignition delay could distort that prediction. The knock resistance of the those blends must therefore be confirmed or falsified in experiments. Pentane exhibits a very high vapor pressure and therefore small quantities of it suffice to meet the vapor pressure restrictions. Hexane is notably more reactive than pentane and at the same time exhibits a lower vapor pressure, rendering it an inferior choice.

Comparison of Predicted Maximum Efficiency to RON, OI, and Merit Function. We compare the predicted engine efficiencies to RON and OI, which are often considered proxies for achievable engine efficiency, and to the engine efficiency merit function of Szybist et al.,[2] which is a linear combination of multiple fuel properties. Figure 9 shows the values of RON, OI, and the merit function in comparison to the efficiency predicted with our model. For the evaluation of OI, we choose a K value of −1 as presumably representative for highly boosted conditions.[10] For the evaluation of the merit function we use K values of both 0 and −1. The values for RON and MON are calculated using linear-by-mole mixing rules.

The merit function requires property values for RON, OS, enthalpy of vaporization, and the laminar burning velocity (LBV) at a pressure of 1.013 25 bar, a temperature of 353 K, and an air−fuel equivalence ratio of 1.1. For RON, OS, and enthalpy of vaporization we use literature data as indicated in Table 3. For the LBV, we use values predicted with the QSPR−ANN by Vom Lehn et al.[80] The merit function requires the assumption of a baseline efficiency with properties of the corresponding reference fuel. Because we use the gasoline surrogate by Sarathy et al.[73] in our model, we use both its properties and its maximum achievable net indicated efficiency as calculated by our engine model (see Table 3) to define the baseline. Following Szybist et al.,[2] the merit function can then be computed as

$$\eta_{\mathrm{merit}} = 38.9\%\left[1 + 0.01\left(\frac{\mathrm{RON} - 96}{1.6} - K\frac{\mathrm{OS} - 7}{1.6} + \frac{0.0085(h_{\mathrm{vap}} - 25\ \mathrm{kJ/kg_{air}})}{1.6} + \frac{h_{\mathrm{vap}} - 25\ \mathrm{kJ/kg_{air}}}{15.2} + \frac{\mathrm{LBV} - 44.4\ \mathrm{cm/s}}{5.4}\right)\right] \quad (24)$$

The plot shows a relatively strong correlation between the efficiency predictions by our model and the RON. The correlation with the OI with a K value of −1 appears to be weaker. Similarly for the merit function, the choice of K impacts the correlation significantly: a K value of 0, denoting no influence of the octane sensitivity, leads to a moderately strong correlation, whereas a value of −1 leads to a rather weak correlation. Note that the different engine configurations associated with each blend resulting from the co-optimization may be representative of different K values. Overall, we conclude that RON is probably the best proxy for engine efficiency as it is predicted by our model.

CONCLUSION

We present an approach to computational co-optimization of fuel and engine. To this end, we derived a thermodynamic engine model based on an ideal engine cycle, largely following standard assumptions and the approach by Gschwend et al.[55] Importantly, our model is applicable to new fuel candidates that have not been tested in an engine yet, as it relies solely on thermophysical property models and ignition delay models fitted to detailed kinetic simulation data. Validation against experimental data from a single-cylinder research engine showed that the model is capable of reproducing trends in efficiency and, with some compromises, the occurrence of engine knock as a function of fuel composition, compression ratio, and intake pressure. We then selected 10 blend stocks on the basis of previous fuel design studies and enumerated binary and ternary blend stock systems. Utilizing the model, we jointly optimized fuel composition, compression ratio for every blend stock system, and intake pressure under consideration of fuel volatility restrictions as well as knock and peak pressure limitations.

The small esters methyl acetate and ethyl acetate are predicted to constitute particularly promising fuel components. They are competitive to small alcohols in terms of knock resistance, but exhibit better volatility characteristics. In contrast to previous computer-aided fuel design studies, the co-optimization does not only identify fuels, but also corresponding engine configurations that may guide subsequent first experimental investigations. For example, methyl-acetate-rich blends are predicted to achieve their maximum engine efficiency at the maximum allowed compression ratio of 20, with the boost pressure limited to 1.8 bar. Moreover, the method predicts whether the efficiency may be limited by peak pressure, knock, or both. The methyl-acetate-rich blends, e.g., are predicted to be not knock limited, even under extreme conditions, but peak pressure limited.

While our study improves upon previous computer-aided fuel design studies by following a fully integrated, computational co-optimization approach, the results are prone to uncertainties caused by the simplifications that were necessary in deriving the engine model. To improve model accuracy, a two-zone model[50] could be implemented, and several submodels need to be improved, namely, the evaporation model, the combustion model, and the knock prediction. The simple evaporation model might cause significant inaccuracies in the calculated temperature profile. A reduced-order droplet model, e.g., the one published by Pu et al.,[81] might constitute an improvement, but it would also require a more detailed gas exchange model and thus increase the computational complexity. The combustion model assumes identical burn profiles for every fuel, although the combustion is influenced by fuel chemistry.[3] A turbulent flame model in combination with correlations for the laminar burning velocity[50] could improve the predicted burn profiles. The knock prediction relies on a linear-by-mole mixing rule for calculating the ignition delay of fuel blends, neglecting potential synergistic combustion kinetic effects altering the knock propensity of multicomponent fuels.

https://doi.org/10.1021/acs.energyfuels.4c04775
Energy Fuels 2025, 39, 4079−4093

Further engine efficiency increases can be achieved by lean combustion.[19] This would however require considering air−fuel-ratio-dependent models of burn profiles and ignition delay time models as well as the lean burn limit of a fuel. Importantly, the model mimics a single-cylinder research engine that is optimized for a single load-point. In the long run, computational co-optimization should consider an actual vehicle engine and consider a wide range of load points as in a driving cycle.

In summary, our study constitutes an important first step in the computational co-optimization of fuel and engine and yielded fuel candidates and recommended engine configurations for subsequent experimental investigations. To further advance the use of thermodynamic engine models in fuel design, considerable modeling efforts will be required.

■ ASSOCIATED CONTENT

Data Availability Statement

The data underlying this study are openly available in our GitLab repository "0D SI engine model for fuel design" at https://git.rwth-aachen.de/avt-svt/public/0d-si-engine-model-for-fuel-design.

Supporting Information

The Supporting Information is available free of charge at https://pubs.acs.org/doi/10.1021/acs.energyfuels.4c04775.

Remaining engine model equations, details on ignition delay time simulations, details on estimation of ignition delay time model parameters, list of all ignition delay time model parameters, derivation of bounds for Wiebe function parameters, and illustration of top 25 ternary blends (PDF)

■ AUTHOR INFORMATION

Corresponding Author

Manuel Dahmen − *Institute of Climate and Energy Systems, Energy Systems Engineering (ICE-1), Forschungszentrum Jülich GmbH, 52425 Jülich, Germany;* orcid.org/0000-0003-2757-5253; Email: m.dahmen@fz-juelich.de

Authors

Philipp Ackermann − *Process Systems Engineering (AVT.SVT), RWTH Aachen University, 52074 Aachen, Germany*

Benjamin Auer − *Process Systems Engineering (AVT.SVT), RWTH Aachen University, 52074 Aachen, Germany*

Patrick Burkardt − *Chair of Thermodynamics of Mobile Energy Conversion Systems (TME), RWTH Aachen University, 52074 Aachen, Germany;* orcid.org/0000-0001-9433-4922

Bastian Lehrheuer − *Chair of Thermodynamics of Mobile Energy Conversion Systems (TME), RWTH Aachen University, 52074 Aachen, Germany*

Philipp Morsch − *Chair of High Pressure Gas Dynamics (HGD), Shock Wave Laboratory, RWTH Aachen University, 52074 Aachen, Germany; Institute for a Sustainable Hydrogen Economy, Process and Plant Engineering for Chemical Hydrogen Storage (INW-4), Forschungszentrum Jülich GmbH, 52425 Jülich, Germany*

Karl Alexander Heufer − *Chair of High Pressure Gas Dynamics (HGD), Shock Wave Laboratory, RWTH Aachen University, 52074 Aachen, Germany;* orcid.org/0000-0003-1657-5231

Stefan Pischinger − *Chair of Thermodynamics of Mobile Energy Conversion Systems (TME), RWTH Aachen University, 52074 Aachen, Germany*

Alexander Mitsos − *JARA-ENERGY, 52056 Aachen, Germany; Process Systems Engineering (AVT.SVT), RWTH Aachen University, 52074 Aachen, Germany; Institute of Climate and Energy Systems, Energy Systems Engineering (ICE-1), Forschungszentrum Jülich GmbH, 52425 Jülich, Germany;* orcid.org/0000-0003-0335-6566

Complete contact information is available at: https://pubs.acs.org/10.1021/acs.energyfuels.4c04775

Author Contributions

Philipp Ackermann and Manuel Dahmen formulated the research gap and scope of the study. Philipp Ackermann derived the engine model with conceptual input from Manuel Dahmen, Patrick Burkardt, and Bastian Lehrheuer. Philipp Ackermann and Benjamin Auer implemented the engine model. Philipp Morsch provided conceptual input for the ignition delay model and software for kinetic simulations. Patrick Burkardt provided the experimental data and conceptual input for parameter estimation and validation. Philipp Ackermann and Manuel Dahmen developed the parameter estimation procedure with conceptual input from Alexander Mitsos. Philipp Ackermann and Benjamin Auer formulated the optimization problem with conceptual input from Alexander Mitsos and Manuel Dahmen. Philipp Ackermann derived the fuel requirements and selected the blend stocks with input from Manuel Dahmen. Alexander Mitsos, Karl Alexander Heufer, and Stefan Pischinger supervised the project. Philipp Ackermann wrote the original draft. All authors reviewed and edited the manuscript and gave their comments for improvements.

Notes

The authors declare no competing financial interest.

■ ACKNOWLEDGMENTS

The authors gratefully acknowledge funding by the Deutsche Forschungsgemeinschaft (DFG, German Research Foundation) under Germany's Excellence Strategy, Cluster of Excellence 2186 "The Fuel Science Center" ID 390919832. Manuel Dahmen received funding from the Helmholtz Association of German Research Centers. The authors kindly thank Sophia Rupprecht for her help in implementing the processing of the thermophysical property data and Sanket Girhe for providing the laminar burning velocity predictions. Furthermore, the authors kindly thank Adrian Schloßhauer for the fruitful discussions about thermodynamic engine modeling.

■ REFERENCES

(1) Kalghatgi, G.; Levinsky, H.; Colket, M. Future transportation fuels. *Prog. Energy Combust. Sci.* **2018**, *69*, 103−105.

(2) Szybist, J. P.; Busch, S.; McCormick, R. L.; Pihl, J. A.; Splitter, D. A.; Ratcliff, M. A.; Kolodziej, C. P.; Storey, J. M.; Moses-DeBusk, M.; Vuilleumier, D.; Sjöberg, M.; Sluder, C. S.; Rockstroh, T.; Miles, P. What fuel properties enable higher thermal efficiency in spark-ignited engines? *Prog. Energy Combust. Sci.* **2021**, *82*, 100876.

(3) Heywood, J. B. *Internal Combustion Engine Fundamentals*; McGraw-Hill: New York, 1988.

(4) Wang, Z.; Liu, H.; Reitz, R. D. Knocking combustion in spark-ignition engines. *Prog. Energy Combust. Sci.* **2017**, *61*, 78−112.

(5) Splitter, D.; Pawlowski, A.; Wagner, R. A historical analysis of the co-evolution of gasoline octane number and spark-ignition engines. *Front. Mech. Eng.* **2016**, *1*, 16.
(6) ASTM International. *Materials Standard Test Method for Research Octane Number of Spark-Ignition Engine Fuel*; ASTM International: West Conshohocken, PA, 2018.
(7) ASTM International. *Materials Standard Test Method for Motor Octane Number of Spark-Ignition Engine Fuel*; ASTM International: West Conshohocken, PA, 2019.
(8) ASTM International. *Materials Standard Specification for Automotive Spark-Ignition Engine Fuel*; ASTM International: West Conshohocken, PA, 2021.
(9) German Institute for Standardization (DIN). *EN 228:2012+A1:2017, Automotive Fuels—Unleaded Petrol—Requirements and Test Methods*; DIN: Berlin, Germany, 2017.
(10) Kassai, M.; Aksu, C.; Shiraishi, T.; Cracknell, R.; Shibuya, M. Mechanism Analysis on the Effect of Fuel Properties on Knocking Performance at Boosted Conditions. *SAE Tech. Pap. Ser.* **2019**, 2019-01-0035.
(11) Kalghatgi, G. T. Fuel Anti-Knock Quality—Part I. Engine Studies. *SAE Tech. Pap. Ser.* **2001**, 2001-01-3584.
(12) Leppard, W. R. The Chemical Origin of Fuel Octane Sensitivity. *SAE Int. J. Fuels Lubr.* **1990**, *99*, 862−876.
(13) Wang, C.; Xu, H.; Daniel, R.; Ghafourian, A.; Herreros, J. M.; Shuai, S.; Ma, X. Combustion characteristics and emissions of 2-methylfuran compared to 2,5-dimethylfuran, gasoline and ethanol in a DISI engine. *Fuel* **2013**, *103*, 200−211.
(14) Hoppe, F.; Burke, U.; Thewes, M.; Heufer, A.; Kremer, F.; Pischinger, S. Tailor-Made Fuels from Biomass: Potentials of 2-butanone and 2-methylfuran in direct injection spark ignition engines. *Fuel* **2016**, *167*, 106−117.
(15) Burkardt, P.; Ottenwälder, T.; König, A.; Viell, J.; Mitsos, A.; Wouters, C.; Marquardt, W.; Pischinger, S.; Dahmen, M. Toward co-optimization of renewable fuel blend production and combustion in ultra-high efficiency SI engines. *International Journal of Engine Research* **2023**, *24*, 29−41.
(16) Ackermann, P.; et al. Designed to Be Green, Economic, and Efficient: A Ketone-Ester-Alcohol-Alkane Blend for Future Spark-Ignition Engines. *ChemSusChem* **2021**, *14*, 5254−5264.
(17) Brusstar, M.; Stuhldreher, M.; Swain, D.; Pidgeon, W. High Efficiency and Low Emissions from a Port-Injected Engine with Neat Alcohol Fuels. *SAE Int. J. Fuels Lubr.* **2002**, *111*, 1445−1451.
(18) Verhelst, S.; Turner, J. W. G.; Sileghem, L.; Vancoillie, J. Methanol as a fuel for internal combustion engines. *Prog. Energy Combust. Sci.* **2019**, *70*, 43−88.
(19) Wouters, C.; Burkardt, P.; Pischinger, S. Limits of compression ratio in spark-ignition combustion with methanol. *International Journal of Engine Research* **2022**, *23*, 793−803.
(20) Feng, H.; Lai, K.; Zheng, Z.; Lin, S.; Wu, X.; Tang, Q. Effects of methanol direct injection and high compression ratio on improving the performances of a spark-ignition passenger car engine. *Fuel* **2024**, *357*, 130052.
(21) Brinkman, N. D. Effect of compression ratio on exhaust emissions and performance of a methanol-fueled single-cylinder engine. *SAE Tech. Pap. Ser.* **1977**, 770791.
(22) Larsen, U.; Johansen, T.; Schramm, J. *Ethanol as a Fuel for Road Transportation*; Technical University of Denmark: Kongens Lyngby, Denmark, 2009; https://amf-tcp.org/app/webroot/files/file/Annex%20Reports/AMF_Annex_35-1.pdf (accessed Aug 29, 2024).
(23) Nithyanandan, K.; Zhang, J.; Li, Y.; Wu, H.; Lee, T. H.; Lin, Y.; Lee, C.-f. F. Improved SI engine efficiency using Acetone−Butanol−Ethanol (ABE). *Fuel* **2016**, *174*, 333−343.
(24) Tang, Q.; Ren, K.; Xie, X.; Chen, T.; Jiang, P.; Zhang, D. The Effect of Acetone-Butanol-Ethanol and Gasoline Blends on the Knocking Performance of Spark-Ignition Engine. *Thermal Science and Engineering Progress* **2023**, *46*, 102175.
(25) Burkardt, P.; Wouters, C.; Pischinger, S. Beating neat fuels by dedicated blending: Performance analysis of bio-hybrid fuel blends on a spark-ignition engine for passenger car applications. *Fuel* **2023**, *331*, 125579.
(26) Hoppe, F.; Heuser, B.; Thewes, M.; Kremer, F.; Pischinger, S.; Dahmen, M.; Hechinger, M.; Marquardt, W. Tailor-made fuels for future engine concepts. *International Journal of Engine Research* **2016**, *17*, 16−27.
(27) McCormick, R. L.; Fioroni, G.; Fouts, L.; Christensen, E.; Yanowitz, J.; Polikarpov, E.; Albrecht, K.; Gaspar, D. J.; Gladden, J.; George, A. Selection Criteria and Screening of Potential Biomass-Derived Streams as Fuel Blendstocks for Advanced Spark-Ignition Engines. *SAE International Journal of Fuels and Lubricants* **2017**, *10*, 442−460.
(28) Leitner, W.; Klankermayer, J.; Pischinger, S.; Pitsch, H.; Kohse-Höinghaus, K. Advanced Biofuels and Beyond: Chemistry Solutions for Propulsion and Production. *Angewandte Chemie (International ed. in English)* **2017**, *56*, 5412−5452.
(29) Zhang, L.; Mao, H.; Liu, Q.; Gani, R. Chemical product design−recent advances and perspectives. *Current Opinion in Chemical Engineering* **2020**, *27*, 22−34.
(30) Dahmen, M.; Marquardt, W. Model-Based Design of Tailor-Made Biofuels. *Energy Fuels* **2016**, *30*, 1109−1134.
(31) Dahmen, M.; Marquardt, W. Model-Based Formulation of Biofuel Blends by Simultaneous Product and Pathway Design. *Energy Fuels* **2017**, *31*, 4096−4121.
(32) König, A.; Siska, M.; Schweidtmann, A. M.; Rittig, J. G.; Viell, J.; Mitsos, A.; Dahmen, M. Designing Production-Optimal Alternative Fuels for Conventional, Flexible-Fuel, and Ultra-High Efficiency Engines. *Chem. Eng. Sci.* **2021**, *237*, 116562.
(33) Vom Lehn, F.; Cai, L.; Tripathi, R.; Broda, R.; Pitsch, H. A property database of fuel compounds with emphasis on spark-ignition engine applications. *Applications in Energy and Combustion Science* **2021**, *5*, 100018.
(34) Cai, G.; Liu, Z.; Zhang, L. Transformation rule-based molecular evolution for automatic gasoline molecule design. *Chem. Eng. Sci.* **2022**, *263*, 118119.
(35) Rittig, J. G.; Ritzert, M.; Schweidtmann, A. M.; Winkler, S.; Weber, J. M.; Morsch, P.; Heufer, K. A.; Grohe, M.; Mitsos, A.; Dahmen, M. Graph Machine Learning for Design of High-Octane Fuels. *AIChE J.* **2023**, *69*, No. e17971.
(36) Vuilleumier, D.; Huan, X.; Casey, T.; Sjöberg, M. Uncertainty Assessment of Octane Index Framework for Stoichiometric Knock Limits of Co-Optima Gasoline Fuel Blends. *SAE International Journal of Fuels and Lubricants* **2018**, *11*, 247−270.
(37) Zhou, Z.; Yang, Y.; Brear, M.; Lacey, J.; Leone, T. G.; Anderson, J. E.; Shelby, M. H. A Comparison of Four Methods for Determining the Octane Index and K on a Modern Engine with Upstream, Port or Direct Injection. *SAE Tech. Pap. Ser.* **2017**, 2017-01-0666.
(38) Kasseris, E.; Heywood, J. B. Charge Cooling Effects on Knock Limits in SI DI Engines Using Gasoline/Ethanol Blends: Part 2-Effective Octane Numbers. *SAE International Journal of Fuels and Lubricants* **2012**, *5*, 844−854.
(39) Leone, T. G.; Anderson, J. E.; Davis, R. S.; Iqbal, A.; Reese, R. A.; Shelby, M. H.; Studzinski, W. M. The Effect of Compression Ratio, Fuel Octane Rating, and Ethanol Content on Spark-Ignition Engine Efficiency. *Environ. Sci. Technol.* **2015**, *49*, 10778−10789.
(40) Zhang, B.; Sarathy, S. M. Lifecycle optimized ethanol-gasoline blends for turbocharged engines. *Applied Energy* **2016**, *181*, 38−53.
(41) Chen, Y.; Zheng, Z.; Lu, Z.; Wang, H.; Wang, C.; Sun, X.; Xu, L.; Yao, M. Machine learning-based screening of fuel properties for SI and CI engines using a hybrid group extraction method. *Applied Energy* **2024**, *366*, 123257.
(42) Nagaraja, S. S.; Sarathy, S. M.; Mohan, B.; Chang, J. Machine learning-driven screening of fuel additives for increased spark-ignition engine efficiency. *Proceedings of the Combustion Institute* **2024**, *40*, 105658.
(43) Fleitmann, L.; Ackermann, P.; Schilling, J.; Kleinekorte, J.; Rittig, J. G.; Vom Lehn, F.; Schweidtmann, A. M.; Pitsch, H.; Leonhard, K.; Mitsos, A.; Bardow, A.; Dahmen, M. Molecular Design

https://doi.org/10.1021/acs.energyfuels.4c04775
Energy Fuels 2025, 39, 4079−4093

of Fuels for Maximum Spark-Ignition Engine Efficiency by Combining Predictive Thermodynamics and Machine Learning. *Energy Fuels* **2023**, *37*, 2213−2229.
(44) Foong, T. M.; Morganti, K. J.; Brear, M. J.; da Silva, G.; Yang, Y.; Dryer, F. L. The Effect of Charge Cooling on the RON of Ethanol/Gasoline Blends. *SAE International Journal of Fuels and Lubricants* **2013**, *6*, 34−43.
(45) Ratcliff, M. A.; Burton, J.; Sindler, P.; Christensen, E.; Fouts, L.; McCormick, R. L. Effects of Heat of Vaporization and Octane Sensitivity on Knock-Limited Spark Ignition Engine Performance. *SAE Tech. Pap. Ser.* **2018**, 2018-01-0218.
(46) Mohanan, P.; Babu, M. G. A simulation model for a methanol fueled turbocharged multi-cylinder automotive spark ignition engine. *SAE Tech. Pap. Ser.* **1991**, 912417.
(47) Shen, Y.; Bedford, J.; Wichman, I. S. Thermodynamic modeling of direct injection methanol fueled engines. *Applied Thermal Engineering* **2009**, *29*, 2379−2385.
(48) Vancoillie, J.; Sileghem, L.; Verhelst, S. Development and validation of a quasi-dimensional model for methanol and ethanol fueled SI engines. *Applied Energy* **2014**, *132*, 412−425.
(49) Nguyen, D.-K.; Suijs, W.; Sileghem, L.; Verhelst, S. Modeling of a methanol fuelled direct-injection spark-ignition engine with reformed-exhaust gas recirculation. *SAE Tech. Pap. Ser.* **2021**, 2021-01-0445.
(50) Verhelst, S.; Sheppard, C. Multi-zone thermodynamic modelling of spark-ignition engine combustion − An overview. *Energy Conversion and Management* **2009**, *50*, 1326−1335.
(51) Perini, F.; Paltrinieri, F.; Mattarelli, E. A quasi-dimensional combustion model for performance and emissions of SI engines running on hydrogen−methane blends. *Int. J. Hydrogen Energy* **2010**, *35*, 4687−4701.
(52) Djouadi, A.; Bentahar, F. Combustion study of a spark-ignition engine from pressure cycles. *Energy* **2016**, *101*, 211−217.
(53) Pourkhesalian, A. M.; Shamekhi, A. H.; Salimi, F. Alternative fuel and gasoline in an SI engine: A comparative study of performance and emissions characteristics. *Fuel* **2010**, *89*, 1056−1063.
(54) Caton, J. A. Implications of fuel selection for an SI engine: Results from the first and second laws of thermodynamics. *Fuel* **2010**, *89*, 3157−3166.
(55) Gschwend, D.; Soltic, P.; Edinger, P.; Wokaun, A.; Vogel, F. Performance evaluation of gasoline alternatives using a thermodynamic spark-ignition engine model. *Sustainable Energy Fuels* **2017**, *1*, 1991−2005.
(56) Gschwend, D.; Soltic, P.; Wokaun, A.; Vogel, F. Review and Performance Evaluation of Fifty Alternative Liquid Fuels for Spark-Ignition Engines. *Energy Fuels* **2019**, *33*, 2186−2196.
(57) The MathWorks, Inc. *MATLAB, Version 9.8.0.1359463 (R2020a)*; The MathWorks, Inc.: Natick, MA, 2020.
(58) Pischinger, R.; Klell, M.; Sams, T. *Thermodynamik der Verbrennungskraftmaschine*; Springer: Vienna, Austria, 2009; DOI: 10.1007/978-3-211-99277-7.
(59) Hohenberg, G. F. Advanced Approaches for Heat Transfer Calculations. *SAE Trans.* **1979**, 2788−2806.
(60) Ghojel, J. I. Review of the development and applications of the Wiebe function: A tribute to the contribution of Ivan Wiebe to engine research. *International Journal of Engine Research* **2010**, *11*, 297−312.
(61) Yeliana, Y.; Cooney, C.; Worm, J.; Michalek, D.; Naber, J. Wiebe function parameter determination for mass fraction burn calculation in an ethanol-gasoline fuelled SI engine. *Journal of KONES* **2008**, *15*, 567−574.
(62) Livengood, J. C.; Wu, P. C. Correlation of autoignition phenomena in internal combustion engines and rapid compression machines. *Fifth Symposium (International) on Combustion* **1955**, *5*, 347−356.
(63) Douaud, A. M.; Eyzat, P. Four-Octane-Number Method for Predicting the Anti-Knock Behavior of Fuels and Engines. *SAE Trans.* **1978**, 294−308.
(64) Vandersickel, A.; Hartmann, M.; Vogel, K.; Wright, Y. M.; Fikri, M.; Starke, R.; Schulz, C.; Boulouchos, K. The autoignition of practical fuels at HCCI conditions: High-pressure shock tube experiments and phenomenological modeling. *Fuel* **2012**, *93*, 492−501.
(65) Jiang, X.; Deng, F.; Yang, F.; Huang, Z. Ignition Delay Characteristics and Kinetic Investigation of Dimethyl Ether/ n -Pentane Binary Mixtures: Interpreting the Effect of the Equivalence Ratio and Dimethyl Ether Blending. *Energy Fuels* **2018**, *32*, 3814−3823.
(66) Singer, A. B.; Taylor, J. W.; Barton, P. I.; Green, W. H. Global Dynamic Optimization for Parameter Estimation in Chemical Kinetics. *J. Phys. Chem. A* **2006**, *110*, 971−976.
(67) Yanowitz, J.; McCormick, R. L. Review: Fuel Volatility Standards and Spark-Ignition Vehicle Driveability. *SAE International Journal of Fuels and Lubricants* **2016**, *9*, 408−429.
(68) Yunus, N. A.; Gernaey, K. V.; Woodley, J. M.; Gani, R. A systematic methodology for design of tailor-made blended products. *Comput. Chem. Eng.* **2014**, *66*, 201−213.
(69) Hart, W. E.; Watson, J.-P.; Woodruff, D. L. Pyomo: modeling and solving mathematical programs in Python. *Mathematical Programming Computation* **2011**, *3*, 219−260.
(70) Caspari, A.; Bremen, A. M.; Faust, J. M. M.; Jung, F.; Kappatou, C. D.; Sass, S.; Vaupel, Y.; Hannemann-Tamás, R.; Mhamdi, A.; Mitsos, A. DyOS—A Framework for Optimization of Large-Scale Differential Algebraic Equation Systems. *29th European Symposium on Computer Aided Process Engineering; Computer Aided Chemical Engineering*; Elsevier: Amsterdam, Netherlands, 2019; Vol. *46*; pp 619−624, DOI: 10.1016/B978-0-12-818634-3.50104-1.
(71) Andersson, J. A. E.; Gillis, J.; Horn, G.; Rawlings, J. B.; Diehl, M. CasADi: a software framework for nonlinear optimization and optimal control. *Mathematical Programming Computation* **2019**, *11*, 1−36.
(72) American Institute of Chemical Engineers (AIChE). *DIPPR 801 Database, Version 12.3.0*; AIChE: New York, 2018; http://www.aiche.org/dippr.
(73) Sarathy, S. M.; et al. Compositional effects on the ignition of FACE gasolines. *Combust. Flame* **2016**, *169*, 171−193.
(74) Naegeli, D. W.; Yost, D. M.; Moulton, D. S.; Owens, E. C.; Chui, G. K. The Measurement of Octane Numbers for Methanol and Reference Fuels Blends. *SAE Int. J. Fuels Lubr.* **1989**, *98*, 712−722.
(75) Yanowitz, J.; Christensen, E.; McCormick, R. L. *Utilization of Renewable Oxygenates as Gasoline Blend Components*; National Renewable Energy Laboratory (NREL): Golden, CO, 2011; Technical Report NREL/TP-5400-50791, http://www.nrel.gov/docs/fy11osti/50791.pdf (accessed Aug 29, 2024).
(76) Derfer, J. M.; Boord, C. E.; Burk, F. C.; Hess, R. E.; Lovell, W. G.; Randall, R. A.; Sabina, J. R. *Knocking Characteristics of Pure Hydrocarbons*; ASTM International: West Conshohocken, PA, 1958.
(77) König, A.; Neidhardt, L.; Viell, J.; Mitsos, A.; Dahmen, M. Integrated design of processes and products: Optimal renewable fuels. *Comput. Chem. Eng.* **2020**, *134*, 106712.
(78) Ahmed, A.; et al. Small ester combustion chemistry: Computational kinetics and experimental study of methyl acetate and ethyl acetate. *Proceedings of the Combustion Institute* **2019**, *37*, 419−428.
(79) Morsch, P.; Döntgen, M.; Heufer, K. A. Kinetic investigations on the high- and low-temperature chemistry of ethyl acetate. *Combust. Flame* **2022**, *243*, 111995.
(80) Vom Lehn, F.; Cai, L.; Copa Cáceres, B.; Pitsch, H. Exploring the fuel structure dependence of laminar burning velocity: A machine learning based group contribution approach. *Combust. Flame* **2021**, *232*, 111525.
(81) Pu, Y.-H.; Dierickx, J.; Verhelst, S. Modelling the evaporative cooling effect from methanol injection in the intake of internal combustion engines. *Fuel* **2024**, *372*, 132131.

https://doi.org/10.1021/acs.energyfuels.4c04775
Energy Fuels 2025, 39, 4079−4093